PATTERN FORMATION IN RAYLEIGH-BÉNARD CONVECTION IN A RAPIDLY ROTATING CYLINDER

Michael Sprague, Keith Julien
Department of Applied Mathematics,
University of Colorado
UCB 526, Boulder, CO 80309-0526, USA
Michael.Sprague@Colorado.edu, Keith.Julien@Colorado.edu

Eric Serre
MSNM-GP UMR6181 CNRS
Universités d'Aix-Marseille I, II & III,
La Jetée Technopôle de Château-Gombert, 38 rue Joliot-Curie, 13451 Marseille cedex 20, France
serre1@l3m.univ-mrs.fr

J.J. Sánchez-Álvarez, E. Crespo del Arco
Departmento Física Fundamental,
U.N.E.D., Apdo. 60.141,28080 Madrid, Spain
jsanchez@bec.uned.es, emi@fisfun.uned.es

ABSTRACT

Pattern formation in a rotating Rayleigh-Bénard convection configuration is investigated for moderate and rapid rotation in moderate aspect-ratio cavities. While the existence of Küppers-Lortz rolls is predicted by theory at the onset of convection (Küppers and Lortz, 1969; Busse and Clever, 1979), square patterns have been observed in physical (Bajaj et al., 1998) and numerical experiments (Sánchez-Álvarez et al., 2005) at relatively high rotation rates. Direct numerical simulation (DNS) of the Boussinesq equations becomes progressively more difficult as the rotation rate is increased due the presence of increasingly thin Ekman boundary layers and fast inertial waves. In addition to presenting numerical results produced from DNS of the full Boussinesq equations, we derive a reduced system of nonlinear PDEs valid for convection in a cylinder in the rapidly rotating limit. Reduced equations have been of great utility in the investigation of rapidly rotating convection on the infinite plane (Julien et al., 1998, 2005; Sprague et al., 2005)

INTRODUCTION

Rotating Rayleigh-Bénard (RB) convection has important applications in geophysical and astrophysical flows as well as industrial applications (Boubnov and Golitsyn, 1995; Knobloch, 1998; Bodenschatz et al., 2000). In this paper, we consider Rayleigh-Bénard convection in a closed cylinder with radius R and height H that is under uniform rotation (with angular velocity Ω) about the vertical axis and has a temperature difference ΔT imposed between the top an bottom surfaces. We focus on pattern formation near the onset of convection and under rapid rotation for $\varepsilon = (\Delta T/\Delta T_c - 1) << 1$ where ΔT_c is the temperature difference at which convective motion sets in. We are primarily interested in the formation of square patterns and Küppers-Lortz (KL) rolls (Küppers and Lortz, 1969; Ecke and Liu, 1998; Ning and Ecke, 1993). KL rolls is a time-dependent state where rolls lose stability to rolls of another orientation. While the existence of KL rolls is predicted by theory (Küppers and Lortz, 1969; Busse and Clever, 1979), precessing square patterns have been observed in physical (Bajaj et al., 1998) and numerical experiments (Sánchez-Álvarez et al., 2005) carried out for cavities with moderate rotation rates and aspect ratios; the formation mechanism is not well understood.

Flow in this configuration is well described by the Boussinesq equations ((Chandrasekhar, 1961)) in a cylindrical coordinate system (r, θ, z):

$$\begin{aligned} D_t\mathbf{u} + E^{-1}\widehat{\mathbf{z}}\times\mathbf{u} &= \overline{P}\nabla p + \widehat{\mathbf{z}}\frac{Ra}{\sigma}T + \nabla^2\mathbf{u} + \mathbf{C} \\ \nabla\cdot\mathbf{u} &= \frac{1}{r}\partial_r(ru) + \frac{1}{r}\partial_\theta v + \partial_z w = 0 \quad (1) \\ D_t T &= \sigma^{-1}\nabla^2 T \end{aligned}$$

where $\mathbf{u} = (u, v, w)^T$, $D_t \equiv \partial_t + \mathbf{u}\cdot\nabla$, p is pressure, $\overline{P}$ is the Euler number, $\sigma = \nu/\kappa$ is the Prandtl number, $E = \nu/(\Omega H^2)$ is the Ekman number, where ν is the kinematic viscosity, κ is the thermal diffusivity, $Ra = g\alpha\Delta T H^3/(\nu\kappa)$, where g is gravity and α is the coefficient of thermal expansion, T is the temperature anomaly,

$$\nabla^2 := \frac{1}{r}\partial_r\left(r\partial_r\right) + \frac{1}{r^2}\partial^2\theta + \partial_z^2$$

$$\mathbf{u}\cdot\nabla := u\frac{\partial}{\partial r} + \frac{v}{r}\frac{\partial}{\partial\theta} + w\frac{\partial}{\partial z}$$

and thus

$$\mathbf{C} = \left(\frac{v^2}{r} - \frac{u}{r^2} - \frac{2}{r^2}\partial_\theta v, -\frac{uv}{r} - \frac{v}{r^2} + \frac{2}{r^2}\partial_\theta u, 0 \right)^T$$

We restrict our investigation to the case where the sidewalls are insulated, and no-slip conditions are employed on all boundaries.

Direct numerical simulation (DNS) of the above system becomes progressively more difficult as the rotation rate is increased:

- Boundary layers on the top and bottom surfaces become increasingly thin as the rotation rate is increased, viz. $\lambda_{bl} \sim \mathcal{O}\left(E^{1/2}\right)$; these must be spatially resolved,
- fast inertial waves exist; these reduce the allowable size of time steps, viz. $\Omega_I \sim \mathcal{O}\left(E^{-1}\right)$.

It is for these reasons that, even with modern computers, DNS of the Boussinesq equations for very large rotation rates ($E \to 0$) is prohibitive if not impossible.

In this paper we discuss recent results (Serre et al., 2003; Sánchez-Álvarez et al., 2005), for slightly supercritical pattern formation in Rayleigh-Bénard convection in a cylinder produced with direct numerical simulation and somewhat large finite rotation rates. In an effort to promote study in the rapidly rotating regime, we introduce a set of equations for RB convection in a cylinder, but derived asymptotically in the limit of rapid rotation. Reduced equations developed in the rapidly rotating limit for RB convection on a plane infinite in the horizontal have shown much success (Julien and Knobloch, 1998; Julien et al., 2005; Sprague et al., 2005) in capturing the important characteristics expected for convection in the rapidly rotating regime. In the rapidly rotating limit, Ekman boundary layers are passive (Julien and Knobloch, 1998), and do not affect the leading-order characteristics of the flow. Further, for $\lambda \lesssim O(E^{1/3})$, the reduced equations filter the fast inertial-gravity waves. It is for these reasons that accurate numerical simulation of the reduced equations can readily be achieved. It is hoped that solutions to the reduced model discussed here, will yield insight into the physics of convection in a rapidly rotating closed cylinder.

DNS FOR FINITE ROTATION RATES

Direct numerical simulation of the full Boussinesq equations (2) in a cylinder is achieved with a Fourier-Galerkin method in the azimuthal direction, which involves one Helmholtz equation for each dependent variable and each Fourier mode. These equations are solved with a pseudo-spectral Collocation-Chebyshev discretization in both the radial and axial directions. Velocity-pressure coupling is achieved with an improved projection scheme; time integration is semi-implicit second-order accurate (Serre and Pulicani, 2001). Initial studies (Sánchez-Álvarez et al., 2005) have found good agreement with experimental results for both bulk (Bajaj et al., 1998) and sidewall modes of convection (Ecke and Liu, 1998; Ning and Ecke, 1993).

Figure 1 shows the sequence of patterns in the "steady" regime for increasing Rayleigh numbers and for $E^{-1} = 548$, $\Gamma = R/H = 5$, $\sigma = 6.4$. The first transition to a convective state is through a sidewall mode (figure 1(a)). The sidewall mode consists of a traveling wave, which is rotating in the retrograde direction. The onset of bulk convection occurs at $Ra = 32870$, which is not the Küppers-Lortz state. Indeed, the bulk convection starts from the cavity center ($r = 0$) and extends filling the bulk as Ra is increased. There exists a range of parameters where this cellular pattern "crystallizes" and forms a square lattice that is rotating in the prograde direction and much slower than the wall mode. These results agree with experiments performed in moderate aspect-ratio cavities (Bajaj et al., 1998). At higher Rayleigh numbers the flow in the cavity becomes turbulent.

Table 1: Characteristics parameters of sidewall convection.

	Ra	Γ	E^{-1}	ω_w	k
Ecke & Liu (1998), Experiments	21380	5	548	-3.5	$\sim$
Ning & Ecke (1993), Experiments	21600	2.5	542	-3.6	4.39
Mercader & Net (2001), lin. ana.	22000	2.5	540	-3.5	3.6
Sánchez *et al.*, (2005), DNS	21380	5	548	-3.8	4.2

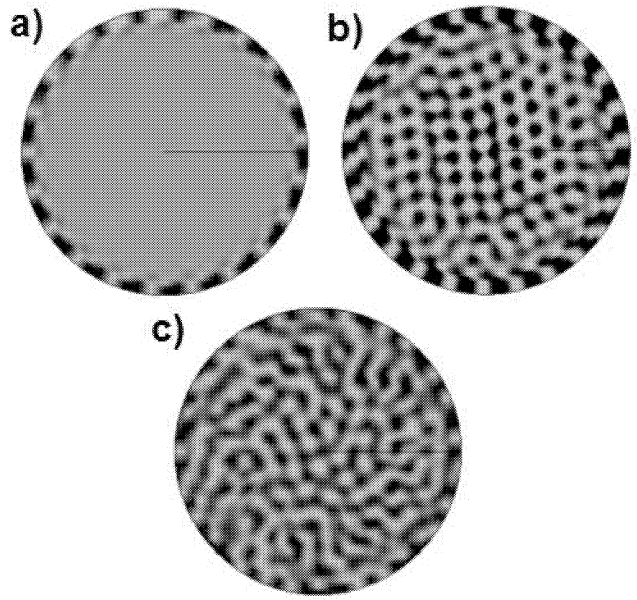

Figure 1: Temperature at mid-height for $E^{-1} = 548$, $\Gamma = 5$, $\sigma = 6.4$. Dark regions are warm up flows and bright regions are cold down flows. (a) $Ra = 21380$: sidewall convection mode, (b) $Ra = 33500$: rotating square pattern convection mode reminiscent of the Küppers-Lortz instability, (c) $Ra = 40000$: spatially disordered pattern.

The main characteristics of sidewall convection are in agreement with experiments (Hermann and Busse, 1993; Ecke and Liu, 1998) and linear stability analysis (Tu and Cross, 1992; Goldstein et al., 1993; Net and Mercader, 2001). In Table 1, the results of the literature are summarized together with the present ones; good agreement is found.

The patterns found in the bulk has similar characteristics to those found by Bajaj et al. (1998). In Table 2 we give the characteristic parameters of the pattern on the bulk. The

angular velocity of the square lattice Ω_{sq} tends to zero with ε going to zero. This indicates that the first bifurcation of the system is not a Hopf bifurcation. It was also found that Ω_{sq} decreases for larger cylinder aspect ratios.

Thus, two modes of convection coexist simultaneously in the cavity. Both are clearly distinguishable in space: the wall mode remains confined near the sidewall, while the square pattern fills the bulk of the cavity. Moreover, their characteristic time scales are vastly different as shown Fig. 2 by the temporal evolution of the temperature; the time behavior is chaotic in the bulk, while it is oscillatory close to the sidewall.

Table 2: Characteristics parameters of bulk convection.

Γ	E^{-1}	σ	Ra_c	Ra	$\Omega_{sq}(d^2/\nu)^{-1}$	k
				33000	0.4×10^{-3}	8.4
5	548	6.4	32870	33500	0.5×10^{-3}	8.5
				34320	$\sim$	8.0
				33000	0.2×10^{-2}	8.4
3	548	6.4	32468	33500	0.5×10^{-2}	8.6
				34320	0.8×10^{-2}	8.9

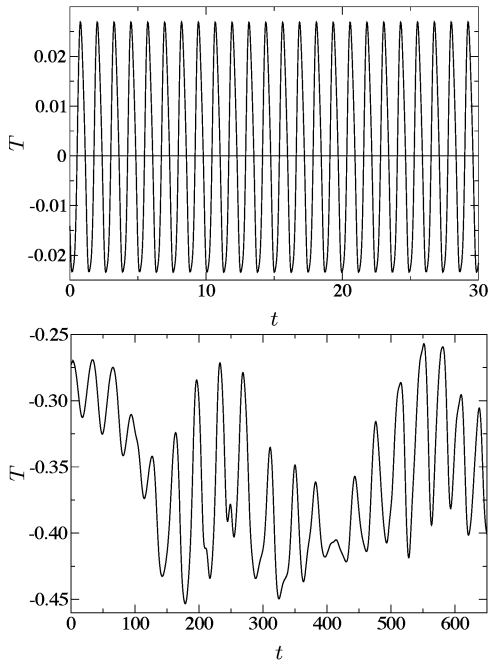

Figure 2: Temporal evolution of the temperature at mid-height for $E^{-1} = 548$, $\Gamma = 5$, and $\sigma = 6.4$ and at a point close to the sidewall (top) and a point in the bulk (bottom).

REDUCED MODEL FOR RAPID ROTATION

As discussed in the Introduction, reduced sets of equations for Rayleigh-Bénard convection in an infinite plane have been developed asymptotically in the limit of rapid rotation ($E \to 0$) (Julien et al., 1998, 2005; Sprague et al., 2005). These reduced equations are appealing for numerical simulation as they filter fast inertial waves and remove the need to resolve Ekman boundary layers, which are passive (Julien and Knobloch, 1998). Direct numerical simulation of the reduced equations have been performed for an infinite plane (Julien et al., 2005; Sprague et al., 2005). For the infinite plane, DNS of the reduced equations is accomplished with a Chebyshev-Tau discretization in the vertical and periodic Fourier modes in the horizontal. Time integration is achieved with a third-order semi-implicit Runge-Kutta algorithm. Figure 2 shows an example simulation result for rapidly rotating convection in an infinite plane.

In this section, we follow the asymptotic derivation of (Sprague et al., 2005), but for Rayleigh-Bénard convection in a closed cylinder with insulated boundary conditions; a more thorough discussion of this derivation may be found in (Julien and Sprague, 2005). For our derivation, we begin with the Boussinesq equations (2), but we use the horizontal length-scale of convection L as our length for nondimensionalization (rather than the cell height H). The resulting momentum equations are

$$D_t\mathbf{u} + A_Z^{-2}E^{-1}\widehat{\mathbf{z}}\times\mathbf{u} = \overline{P}\nabla p + \frac{Ra}{A_Z^3 Pr}T\widehat{\mathbf{z}} + \nabla^2\mathbf{u} + \mathbf{C} \qquad (2)$$

where $A_Z = H/L$; the form of the temperature and continuity equations are unchanged. Following (Julien et al., 2005; Sprague et al., 2005), we employ a multiple-scales expansion in space and time. We introduce a large scale $Z = A_Z^{-1}z$, over which the columns are modulated (cell height; $0 \le Z \le 1$), and $\tau = A_\tau^{-1}t$, is a slow time ($A_Z, A_\tau \gg 1$). We therefore employ the substitutions

$$\partial_z \to \partial_z + \frac{1}{A_Z}\partial_Z, \quad \partial_t \to \partial_t + \frac{1}{A_\tau}\partial_\tau$$

to yield

$$\begin{aligned}(D_t + \frac{1}{A_\tau}\partial_\tau)\mathbf{u} + \frac{w}{A_Z}\partial_Z\mathbf{u} + A_Z^{-2}E^{-1}\widehat{\mathbf{z}}\times\mathbf{u} = -\overline{P}\nabla p \\ -\frac{\overline{P}}{A_Z}\partial_Z p + \frac{Ra}{A_Z^3 Pr}T\widehat{\mathbf{z}} + \nabla^2\mathbf{u} + A_Z^{-2}\partial_Z^2\mathbf{u} + \mathbf{C}\end{aligned}$$

$$(D_t + \frac{1}{A_\tau}\partial_\tau)T + \frac{w}{A_Z}\partial_Z T = Pr^{-1}\left(\nabla^2 T + A_Z^{-2}\partial_Z^2 T\right) \qquad (3)$$

$$\nabla\cdot\mathbf{u} + A_Z^{-1}\partial_Z w = 0$$

By taking the average of the continuity equation (3c) over fast-time and small-spatial scales, we find $\partial_Z\overline{w} = 0$, which implies $\overline{w} = 0$ due to impenetrable boundary conditions, and where the overbar defines the averaging operation

$$\begin{aligned}\overline{f}(Z,\tau) \quad = \quad & \lim_{\tilde{t},\tilde{z}\to\infty}\frac{1}{\tilde{t}\tilde{z}2\pi R}\times \\ & \int_{\tilde{t},\tilde{z}}\int_0^{2\pi}\int_0^R f(r,\theta,z,Z,t,\tau)r\mathrm{d}r\mathrm{d}\theta\mathrm{d}z\mathrm{d}t \qquad (4)\end{aligned}$$

Applying the average operation to the temperature equation (3b), we find

$$A_\tau^{-1}\partial_\tau\overline{T} + A_Z^{-1}\partial_Z\overline{(Tw)} = Pr^{-1}A_Z^{-2}\partial_Z^2\overline{T} \qquad (5)$$

where we have utilized $\partial_r T|_R = 0$ (insulated sidewalls). Assuming $T = \overline{T}(\tau, Z) + T'(\mathbf{x}, Z, t, \tau)$ in (3), where $\overline{T'} = 0$, and subtracting the mean-temperature equation (5), we find the

fluctuating-temperature governing equation

$$(D_t + \frac{1}{A_\tau}\partial_\tau)T' + \frac{w}{A_Z}\partial_Z(\overline{T}+T') - A_Z^{-1}\partial_Z\overline{(Tw)} = \quad (6)$$

$$Pr^{-1}\left(\nabla^2 T' + A_Z^{-2}\partial_Z^2 T'\right) \quad (7)$$

Averaging the vertical-momentum equation in (3) yields

$$A_Z^{-1}\partial_Z\overline{w^2} = -A_Z^{-1}\overline{P}\partial_Z\overline{p} + \frac{Ra}{A_Z^3 Pr}\overline{T} + \gamma \quad (8)$$

where

$$\gamma(\tau, Z) = \lim_{\tilde{t},\tilde{z}\to\infty}\frac{1}{\tilde{t}\tilde{z}2\pi R}\int_{\tilde{t},\tilde{z}}\int_0^{2\pi} R\,\partial_r w|_R\,\mathrm{d}\theta\mathrm{d}z\mathrm{d}t$$

We subtract (8) from the vertical-momentum equation in (3) to yield

$$\left(D_t + \frac{1}{A_\tau}\right)w + \frac{w}{A_Z}\partial_Z w - \frac{1}{A_Z}\partial_Z\overline{w^2} = \overline{P}\left(-\partial_z p - A_Z^{-1}\partial_Z(p-\overline{p})\right) + \frac{Ra}{A_Z^3 Pr}T' + \nabla^2 w + A_Z^{-2}\partial_Z^2 w - \gamma \quad (9)$$

where we have utilized $\overline{w} = 0$.

Following (Julien et al., 2005; Sprague et al., 2005), we expand dependent variables $\mathbf{v} = (\mathbf{u}, p, \overline{T}, T')^T$ in terms of the small parameter $\epsilon \equiv E^{1/3}$

$$\mathbf{v} = \mathbf{v}_0 + \epsilon\mathbf{v}_1 + \epsilon^2\mathbf{v}_2 + O(\epsilon^3), \quad (10)$$

and, without loss of generality, choose the scalings

$$A_Z = \epsilon^{-1}, \quad A_\tau = \epsilon^{-2}, \quad Ra = \epsilon^{-4}\widetilde{Ra} \quad (11)$$

where the scaled Rayleigh number $\widetilde{Ra}$ is an $O(1)$ quantity. Note that this is the scaling selected by linear theory Chandrasekhar (1961). From the mean-temperature equation (5), we find at $O(1)$

$$\partial_Z\left(\overline{T_0' w_0}\right) = 0 \quad (12)$$

where we have utilized $\overline{w} = 0$. As with the upright, infinite-domain case (Sprague et al., 2005), we take $T_0' = 0$ because the choice of $w_0 = w_0' = 0$ would preclude the convective flow dynamics that we are interested in. At $O(\epsilon)$, we find from the mean-temperature equation

$$\partial_\tau\overline{T}_0 + \partial_Z\overline{\left(T_1' w_0\right)} = Pr\partial_Z^2\overline{T}_0$$

where we have utilized $T_0' = 0$, and the fluctuating-temperature equation at $O(\epsilon)$ is

$$D_t^0 T_1' + w_0\partial_Z\overline{T}_0 = Pr^{-1}\nabla^2 T_1' \quad (13)$$

From the average-vertical-momentum equation (8) we find that $\overline{P} = O(\epsilon^{-2})$ for leading-order hydrostatic balance. Further, we take $\overline{P} = \epsilon^{-2}\widetilde{Ra}/Pr$ to yield

$$\partial_Z\overline{p}_0 = \overline{T}_0 \quad (14)$$

If we consider the momentum equation (3a), we find at $O(\epsilon^{-2})$

$$\nabla p_0 = 0$$

and at $O(\epsilon^{-1})$ we obtain the geostrophic balance

$$\widehat{\mathbf{z}}\times\mathbf{u}_0 = -\frac{\widetilde{Ra}}{Pr}\nabla p_1$$

Finally, at $O(\epsilon^0)$ we find

$$\begin{aligned} D_t^0\mathbf{u}_0 + \widehat{\mathbf{z}}\times\mathbf{u}_1 &= -\frac{\widetilde{Ra}}{Pr}\nabla p_2 + \left[-\partial_Z\left(p_1 - \overline{p}_1\right)T_1'\right]\frac{\widetilde{Ra}}{Pr}\widehat{\mathbf{z}} \\ &+ \nabla^2\mathbf{u}_0 + \mathbf{C}_0 - \gamma_0\widehat{\mathbf{z}} \end{aligned}$$

In summary, the resulting closed system is

$$\begin{aligned} \nabla\cdot\mathbf{u}_0 &= 0 \\ \nabla\cdot\mathbf{u}_1 + \partial_Z w_0 &= 0 \\ \widehat{\mathbf{z}}\times\mathbf{u}_0 &= -\frac{\widetilde{Ra}}{Pr}\nabla p_1 \\ D_t^0 T_1' + w_0\partial_Z\overline{T}_0 &= Pr^{-1}\nabla^2 T_1' \\ \partial_\tau\overline{T}_0 + \partial_Z\overline{T_1' w_0} &= Pr^{-1}\partial_Z^2\overline{T}_0 \\ \partial_Z\overline{p}_0 &= \overline{T}_0 \\ D_t^0\mathbf{u}_0 + \widehat{\mathbf{z}}\times\mathbf{u}_1 &= -\frac{\widetilde{Ra}}{Pr}\nabla p_2 - \gamma_0\widehat{\mathbf{z}} + \nabla^2\mathbf{u}_0 \\ &+ \left[-\partial_Z\left(p_1 - \overline{p}_1\right) + T_1'\right]\frac{\widetilde{Ra}}{Pr}\widehat{\mathbf{z}} + \mathbf{C}_0 \end{aligned} \quad (15)$$

It can readily be shown from (15a,c) that all dependent variables obey the Taylor-Proudman theorem (Proudman, 1916; Taylor, 1923) in that they are invariant in the small-scale vertical direction, *i.e.*, $\partial_z \equiv 0$. From (15a) the flow is horizontally non-divergent. However, w_0 remains $O(1)$.

Following Sprague et al. (2005), we incorporate a stream-function formulation where the leading-order velocity is given by

$$\mathbf{u}_0 = \left(-\frac{1}{r}\partial_\theta\psi, \partial_r\psi, \nabla_\perp^2\phi\right)^T$$

where $\nabla_\perp = \left(\partial_r, r^{-1}\partial_\theta, 0\right)^T$. Under this formulation,

$$p_1 = \frac{Pr}{\widetilde{Ra}}\psi$$

Similar to quasigeostrophic flows (Salmon, 1998) pressure is the geostrophic stream-function. It is this constraint that is responsible for filtering the fast inertial waves discussed above.

By applying $\widehat{\mathbf{z}}\cdot$ to the (15g), we find

$$\partial_t\nabla_\perp^2\phi + J\left(\psi, \nabla_\perp^2\phi\right) + \partial_Z\left(\psi - \overline{\psi}\right) = \frac{\widetilde{Ra}}{Pr}T_1' + \nabla_\perp^4\phi - \gamma_0 \quad (16)$$

where $J(f,g) = \frac{1}{r}\partial_r f\partial_\theta g - \frac{1}{r}\partial_\theta f\partial_r g$ is the Jacobian. Finally, applying $\widehat{\mathbf{z}}\cdot\nabla\times$ to the momentum equation, we find after some algebra

$$\partial_t\nabla_\perp^2\psi + J\left(\psi, \nabla_\perp^2\psi\right) - \partial_Z\nabla_\perp^2\phi = \nabla_\perp^4\psi \quad (17)$$

where $\nabla_\perp^2\psi$ is the leading-order vertical vorticity. It is interesting to note that the terms in $\mathbf{C}_0$ collapse into the the Jacobian term or the Laplacian (appendix E in (Petersen,

2004)). Finally, the temperature equations are

$$\begin{aligned} \partial_t T_1' + J\left(\psi, T_1'\right) + \nabla_\perp^2 \phi \partial_Z \overline{T} &= Pr^{-1} \nabla_\perp^2 T_1' \\ \partial_\tau \overline{T}_0 + \partial_Z \overline{T_1' \nabla_\perp^2 \phi} &= Pr^{-1} \partial_Z^2 \overline{T}_0 \end{aligned} \quad (18)$$

Equations (16–18) constitute a closed system. Note that vertical diffusion in (16–18) does not appear because it is sub-dominant. It is this property that relaxes the need to resolve the Ekman boundary layers at the horizontal plates. However, Stewartson layers ($\lambda \sim O(E^{1/4})$; Pedlosky (1987)) at the vertical sidewalls are contained within this reduction which resolves all motions greater than $O(E^{1/3})$.

It is interesting to note that the form of the system (16–18) is very similar to that for an infinite plane (Sprague et al., 2005), where there is no γ_0 and $\mathbf{u}$ is composed only of fluctuating quantities. A further discussion of the above derivation and numerical solution may be found in a future publication (Julien and Sprague, 2005).

In summary, we believe that the reduced equation set reported in (16-18) are advantageous over the Boussinesq equations (2), which have prohibitive spatio-temporal resolution requirements as $E \to 0$.

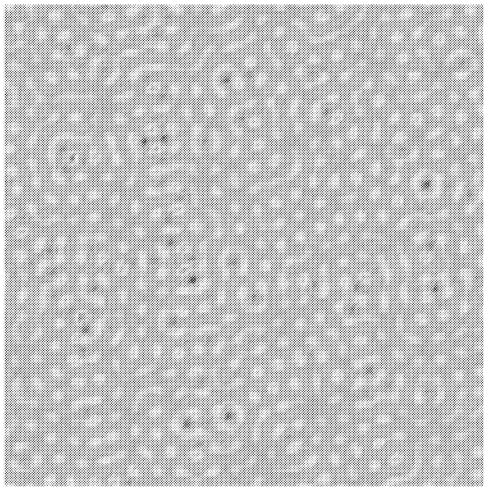

Figure 3: Representative results for temperature at the midplane of an *infinite* plane with $\varepsilon = 0.03$ and $Pr = 6.4$. Dark regions are warm upflows and bright regions are cold downflows. Results were produced with DNS of the reduced equations derived for $E \to 0$ (Sprague et al., 2005; Julien et al., 1998). The spatial grid is composed of 33 Chebyshev modes in the vertical and 128^2 Fourier modes in the horizontal.

*

References

Bajaj, K., J. Liu, B. Naberhuis, and G. Ahlers (1998). Square patterns in Rayleigh-Bénard convection with rotation about a vertical axis. *Physical Review Letters 81*(4), 806–809.

Bodenschatz, E., W. Pesch, and G. Ahlers (2000). Recent developments in Rayleigh-Bénard convection. *Annual Review of Fluid Mechanics 32*, 709–778.

Boubnov, B. and G. Golitsyn (1995). *Convection in Rotating Fluids*. Kluwer Academic Publishers.

Busse, F. and R. Clever (1979). Nonlinear properties of convection rolls in a horizontal layer rotating about a vertical axis. *Journal of Fluid Mechanics 94*, 609–627.

Chandrasekhar, S. (1961). *Hydrodynamic and Hydromagnetic Stability*. Oxford University Press.

Ecke, R. and Y. Liu (1998). Travelling wave and vortex states in rotating Rayleigh-Bénard convection. *International Journal of Engineering Science 36*, 1471–1480.

Goldstein, H., E. Knobloch, I. Mercader, and M. Net (1993). Convection in a rotating cylinder. part 1: Linear theory for moderate Prandtl numbers. *Journal of Fluid Mechanics 248*, 1421–1450.

Hermann, J. and F. Busse (1993). Asymptotic theory of wall-attached convection in a rotating fluid layer. *Journal of Fluid Mechanics 255*, 183–194.

Julien, K. and E. Knobloch (1998). Strongly nonlinear convection cells in a rapidly rotating fluid layer. *Journal of Fluid Mechanics 360*, 141–178.

Julien, K., E. Knobloch, R. Milliff, and J. Werne (2005). Hierarchical models for spatially anisotropic rotationally constrained flows. *Journal of Fluid Mechanics*. Accepted for publication.

Julien, K., E. Knobloch, and J. Werne (1998). A new class of equations for rotationally constrained flow. *Theoretical and Computational Fluid Dynamics 11*, 251–261.

Julien, K. and M. Sprague (2005). Rayleigh-Bénard convection in a rapidly rotating cylinder. In preparation.

Knobloch, E. (1998). Rotating convection: Recent developments. *International Journal of Engineering Science 36*, 1421–1450.

Küppers, G. and D. Lortz (1969). Transition from laminar convection to thermal turbulence in a rotating fluid layer. *Journal of Fluid Mechanics 35*, 609–620.

Net and Mercader (2001). Private communication.

Ning, L. and R. Ecke (1993). Rotating Rayleigh-Bénard convection: Aspect ratio dependence of the initial bifurcations. *Physical Review E 47*, 3326–3334.

Pedlosky, J. (1987). *Geophysical Fluid Dynamnics* (2nd ed.). Springer-Verlag.

Petersen, M. (2004). *A Study of Geophysical and Astrophysical Turbulence using Reduced Equations*. Ph. D. thesis, University of Colorado at Boulder.

Proudman, J. (1916). On the motion of solids in a liquid possessing vorticity. *Proc. R. Soc. London Ser. A 92*, 408–424.

Salmon, R. (1998). *Lectures on Geophysical Fluid Dynamnics*. Oxford University Press.

Sánchez-Álvarez, J., E. Serre, E. Crespo del Arco, and F. Busse (2005). Square patterns in rotating Rayleigh-Bénard convection. *Physical Review E*. Submitted for review.

Serre, E., E. Crespo del Arco, and F. Busse (2003). Transition to chaotic patters in Rayleigh-Bénard convection in a rotating cylinder, nonlinear dynamics in fluids. In *Nonlinear Dynamics in Fluids*, pp. 138–140. CIMNE, Barcelona.

Serre, E. and J. Pulicani (2001). A three-dimensional pseudospectral method for rotating flows in a cylinder. *Computers and Fluids 30*, 491–519.

Sprague, M., K. Julien, E. Knobloch, and J. Werne (2005). Numerical simulation of an asymptotically reduced set of equations for rotationally constrained convection. *Journal of Fluid Mechanics*. Submitted for review.

Taylor, G. (1923). Experiments on the motion of solid bodies in rotating fluids. *Proc. R. Soc. London Ser. A 104*, 213–218.

Tu, Y. and M. Cross (1992). Chaotic domain structure in rotating convection. *Physical Review Letters 69*(17), 2215–2219.